# Complementary use of wind lidars and land-based met-masts for wind measurements in a wide fjord

**E. Cheynet[1]; J. B. Jakobsen[1], J. Snæbjörnsson[1,2], H. Ágústsson[3], K. Harstveit[3]**

[1] Department of Mechanical and Structural Engineering and Materials Science, University of Stavanger, Norway
[2] School of Science and Engineering, Reykjavík University, Iceland
[3] Kjeller Vindteknikk, Kjeller, Norway

E-mail: etienne.cheynet@uis.no

**Abstract.** Wind velocity data recorded on the shores of a wide fjord (Bjørnafjord, Norway) by sonic anemometers mounted on met-masts are compared with those obtained using synchronized long-range lidar instruments. The goal is to know to what extent measurements from land-based met-mast are representative of the wind conditions in the middle of the fjord. The lidar data shows a good agreement with the anemometer records for a limited number of sectors only, indicating a significant influence of the topography on the data obtained on the met-masts. For a north-northwest wind, which was the dominant wind direction during the measurement period, the influence of the local topography on the estimated turbulence characteristics may not be negligible for three of the four masts deployed. This implies that the combined use of remote sensing technology and land-based sensors may be necessary to characterize the wind conditions in a wide fjord.

## 1. Introduction

The future ferry-free coastal route E39 is an ambitious plan led by the Norwegian government to develop the economy of western Norway [1]. Crossing the Bjørnafjord, south of Bergen, with a bridge will be particularly challenging. At the crossing location (Figure 1), the fjord is 5 km wide and up to 500 m deep, so that a feasible solution relies on a floating bridge. The design of such a large structure requires a detailed description of the environmental loads. The study of wind conditions inside the fjord cannot be easily assessed using traditional anemometers. The deployment of anemometers on met-masts on the shores of the fjord provides wind measurements that may be affected by local topographic effects [2,3], especially at the sea-land discontinuity [4–7], which in the case of a fjord may correspond to a sharp escarpment.

An alternative approach relies on the use of Doppler wind lidar (DWL) technology to remotely measure the wind characteristics in the fjord from devices installed on land. The application of DWLs in wind engineering is relatively recent [3, 8] as they have been more frequently used for wind energy applications or atmospheric research [9–11]. From May to June 2016, three synchronized Doppler wind lidars were deployed on the south-west side of the Bjørnafjord (Figure 1) to study the wind conditions in a horizontal plane at a distance of at least 1.6 km from the nearest shore [12]. The analysis of the lidar data in Ref. [12] suggested that for the period considered, the roughness length in the fjord is similar to that of a calm open sea surface.

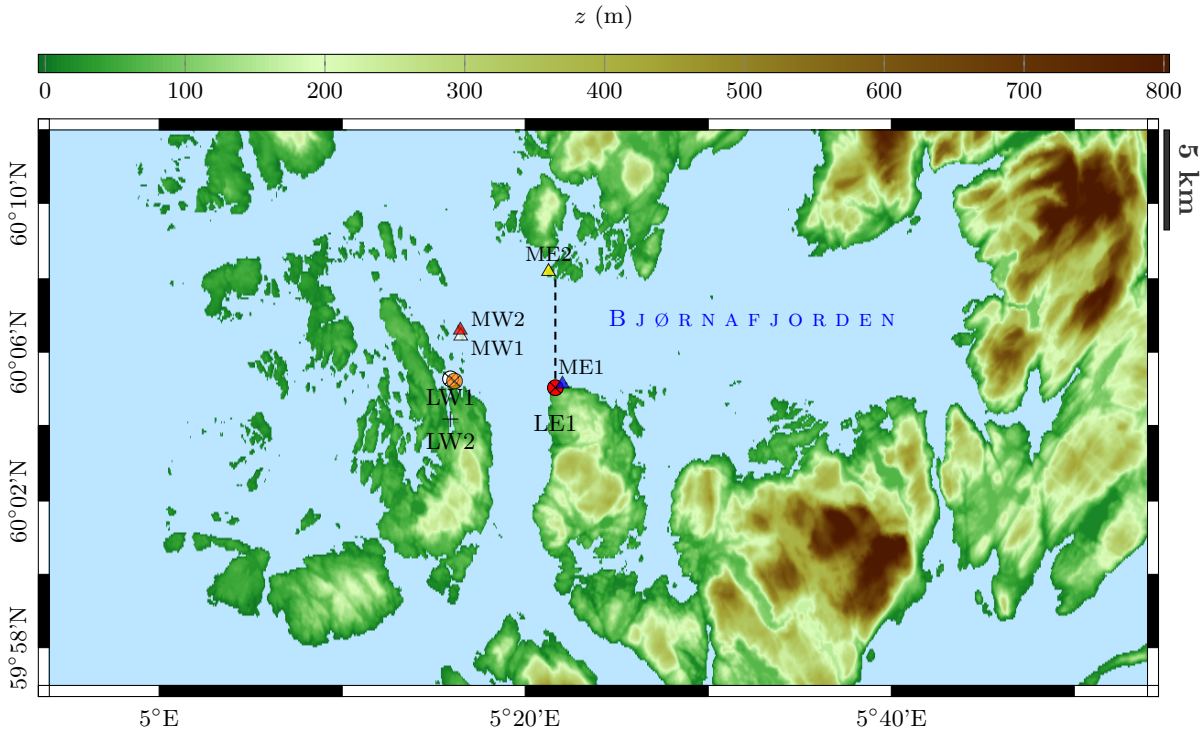


Figure 1: Digital elevation map of the Bjørnafjord showing the location of the three pulsed wind lidars LW1, LW2 and LE1 (circles) and the met masts ME1, ME2, MW1 and MW2 installed by KVT (triangles). The dashed line refers to the planned fjord crossing.

The analysis done in Ref. [12] is here extended using sonic anemometer records from several met-masts installed by Kjeller Vindteknikk (KVT, Norway) [13] for the Norwegian Public Road Administration, on the shores of the Bjørnafjord since 2015 (Figure 1). The novelty of the present study relies on the combination of in-situ measurements from multiple synchronized scanning lidars with anemometer records from the seaside and their analysis. The goal is (1) to assess the level of consistency between the anemometer records and those from the lidar instruments; (2) to discover to what extent the wind velocity data on the shores of the fjord are affected by the surrounding environment.

The present study is organized as follows: Section 2 describes the sonic anemometers on each met-mast as well as the lidar instruments. Section 3 compares the mean wind statistics and the standard deviation of the along-wind component recorded by the sonic anemometers and the lidars. section 4 discusses the influence of the local topography on the sonic anemometer records through the analysis of the one-point turbulence statistics.

## 2. Instrumentation

Four met-masts were installed in the Bjørnafjord by KVT in 2015. Two of them, named MW1 and MW2, are located on Ospøya island (panel **(a)** of Figure 2), at an altitude of 34 m and 23 m above the sea level (asl), respectively. The third mast, denoted ME1, is positioned ca. 9 m asl, on a smaller and flatter island named Svarvhelleholmen (panel **(b)** of Figure 2). The fourth mast, named ME2, is located on the north side of the fjord, at 26 m asl (panel **(d)** of Figure 2). In addition to the irregular terrain around the met-masts, the vegetation differs greatly from one location to another. Around the masts MW1 and MW2, low bushes are dominant with some few trees irregularly spaced. The mast ME1 is mounted in an irregular clearcut, in such a way that

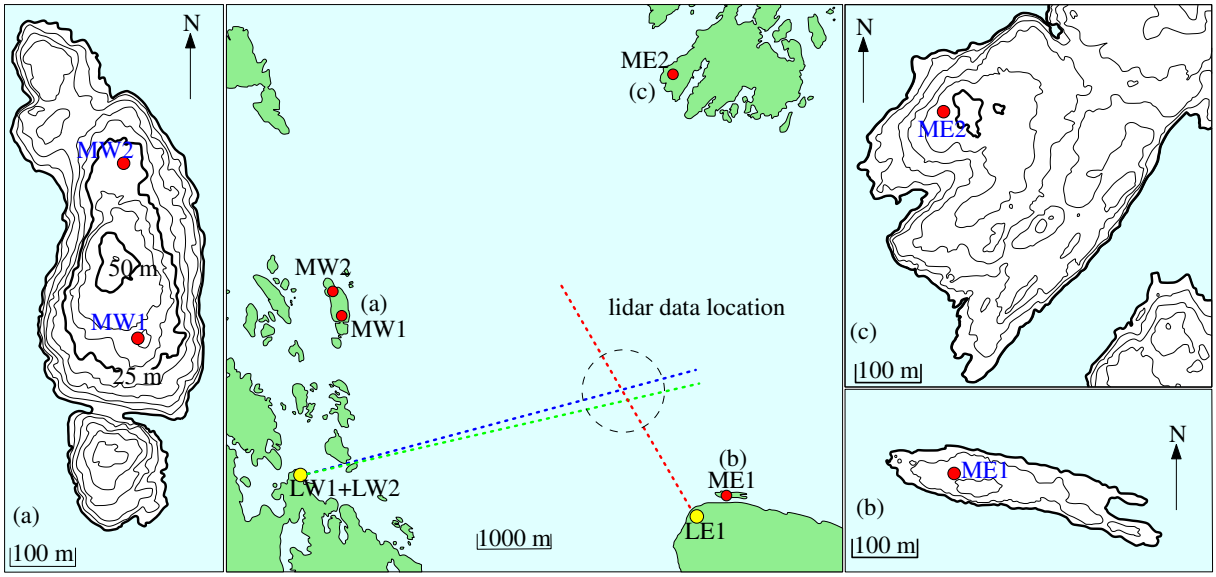


Figure 2: Elevation map of the island of Ospøya **(a)**, Svarvhelleholmen **(c)** and Synnøytangen **(d)**. In panels **(a)**, **(b)** and **(c)**, each contour corresponds to a height of 5 m.

no tree is located on the north side of the mast. The mast ME2 is also located in a clearcut but remains surrounded by a conifer forest.

The masts are 50 m high and have a tubular structure with a diameter up to 25 cm. Three of them are equipped with three sonic anemometers, denoted A, B and C, the altitude of which is summarized in Table 1. During the measurement period considered, the mast MW1 was instrumented with two sonic anemometers only. On the mast MW1 and MW2, the anemometers are mounted on 4 m-long booms oriented with an angle of $-8°$ and $-2°$ from the North, respectively. On the masts ME1 and ME2, the boom length is 2.2 m at the lowest height and 1.8 m at the other two heights. On the mast ME1, the booms are oriented with angles between 1° and 16° from the north, whereas this angle is between 193° and 201° on the mast ME2. The anemometers are Gill WindMaster Pro 3-axis anemometers, configured to record the three wind components with a sampling frequency of 10 Hz. The sonic temperature was, however, not available in the data set used for the present study.

The first lidar unit, named LE1 in Figure 1, is located 25 m asl whereas the two other ones, denoted LW1 and LW2, are ca. 2 m asl. The lidars are WindCube 200S (Leosphere, France), modified by the Technical University of Denmark (DTU, Denmark) and synchronized in a so-called WindScanner system [14]. Each lidar uses an elevation angle equal or lower than 0.3°, such that the scanning pattern at the intersection of the beams is assumed horizontal and at 25 m asl. In the present study, the along-wind component is retrieved using the along-beam velocity components of the combined lidars LE1 and LW2 with a sampling frequency of 0.22 Hz. Consequently, the WindScanner system records the flow at a lower time resolution than the sonic anemometers (Figure 3). The rotating head of the lidar LE1 and LW2 scans the flow with an azimuth angle ranging from 324° to 330°, and from 76° to 78°, respectively. The lidar data are collected where the scanning beams intersect, i.e. at a line-of-sight distance of 1.7 km and 4.6 km from the lidars LE1 and LW2, respectively. More details about the lidar instrumentation are given in Ref. [12].

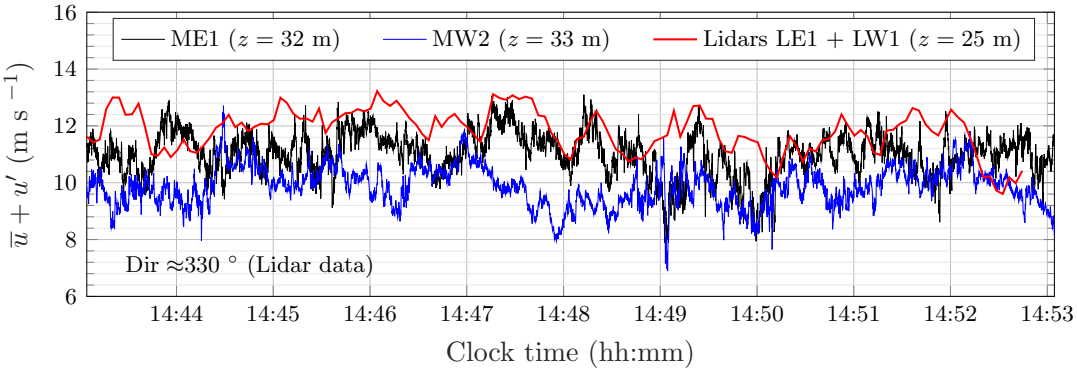


Figure 3: Along wind velocity recorded on 2016-06-09 for a wind direction of 330° and a mean wind velocity of 12 m s$^{-1}$. The measurement height indicated in the legend is the one above the ground.

Table 1: Height of the different sonic anemometers on each mast in the Bjørnafjord.

| | Height above ground (m) | | | Height above sea level (m) | | |
|---|---|---|---|---|---|---|
| Anemometer | A | B | C | A | B | C |
| MW1 | – | 49 | 33 | – | 83 | 67 |
| MW2 | 49 | 49 | 33 | 72 | 72 | 56 |
| ME1 | 48 | 32 | 13 | 57 | 42 | 22 |
| ME2 | 48 | 32 | 13 | 74 | 59 | 39 |

*2.1. Data processing*

The along-wind ($x$-axis), crosswind ($y$-axis) and vertical (positive $z$-axis) wind components are denoted $u$, $v$ and $w$, respectively [15]. Each wind component can be expressed as the sum of a mean component, denoted by an overline and a fluctuating component with zero mean denoted by a prime, such that for the component $j = \{u, v, w\}$, one can write $j = \overline{j} + j'$. The fluctuating component, is assumed to be a stationary Gaussian random process. The standard deviation of the wind component $j = \{u, v, w\}$, is denoted $\sigma_j$ and the corresponding turbulence intensity $I_j$ is defined as:

$$I_j = \frac{\sigma_j}{\overline{u}} \tag{1}$$

For a neutral atmosphere, the Eurocode [16] proposes the following formulation to model the variation of $I_u$ with $z$ and $z_0$, assuming a turbulence factor $k_l$ and an orography factor $c_o$, equal to 1.0:

$$I_u(z) = \begin{cases} \dfrac{1}{\ln\left(z/z_0\right)} & \text{if } z > z_{\min}. \\ I_u(z_{\min}) & \text{if } z \leq z_{\min}. \end{cases} \tag{2}$$

where $z_{\min}$ is the minimum height above which the vertical profile of mean wind velocity follows the logarithmic law. Eq. 2 is established from the logarithmic mean wind velocity profile, assuming that $u_* = \kappa\sigma_u$. If the value $\kappa = 0.40 \pm 0.01$ is taken, as advised in Ref. [17], the ratio $\sigma_u/u_* = 2.5$, used in the literature since the 1960s [18], is found.

For a horizontal flow, only the along-wind component, which is parallel to the mean wind direction ($x$-axis), is assumed to have a non-zero mean value, i.e. $\overline{w} \approx \overline{v} \approx 0\,\mathrm{m\,s^{-1}}$. This means that the incidence angle defined as:

$$\theta = \arctan\left(\frac{w}{u}\right) \tag{3}$$

has a mean value $\overline{\theta}$ equal to 0°, which is not necessarily the case for a complex terrain. For gentle hills, the wind velocity data are often studied in the "streamline coordinate system" [19–21], where $\overline{w} = \overline{v} \approx 0\,\mathrm{m\,s^{-1}}$. This can be done using a sector planar fit (SPF) [22, 23], which relies on the determination of the local terrain slope from a set of several mean wind velocity estimates and a limited wind sector. Another possibility is the use of the double or triple rotation technique [24], which is applied to each sample by minimizing first $\overline{w}$ and then $\overline{v}$. In Section 3, the sonic anemometer data are studied after application of the double rotation technique. Note that the horizontal flow characteristics retrieved this way are nearly the same as those obtained in the Cartesian coordinate system.

In the following, wind statistics are derived using a 10 min averaging time. Although a longer duration is preferable to estimate turbulence characteristic with a better accuracy, the chosen averaging time is consistent with the one used in Ref. [12], where the data processing of the lidar data is the same as done in the present study.

One-point turbulence characteristics are studied after de-spiking and removing the linear trend. In section 4, non-stationary wind fluctuations are in addition disregarded, which are identified using the reverse arrangement test [25], applied to velocity fluctuations with a frequency equal to or lower than 0.25 Hz and a 95 % confidence interval. Note that the stationarity test is applied to the de-trended velocity fluctuations, which is an appropriate choice in Section 4 where only the fluctuating wind velocity component is investigated.

In Ref. [12], the lidar data were divided into two subsets corresponding to two different scanning configurations. In the present study, the two subsets are merged. For each sonic anemometer, the data availability is larger than 99 % whereas it is ca. 46 % for the lidar instruments. In section 3, where the lidar and anemometer records are compared, the two data sets are collocated in time, such that only $3.8 \times 10^3$ samples of 10 min duration are used. In section 4, only on the wind measurements from the anemometers are considered, allowing the use of a much larger data set since it is no longer limited by the data availability of the lidar records.

## 3. Inter-comparison of the anemometer and lidar data

The wind records used in Figure 4 correspond to the lidar data recorded 25 m above sea level, ca. 1.7 km on the north of the mast ME1, and those from the sonic anemometers at a height of 32 m − 33 m above ground. Figure 4 shows that when the lidar data are available, the dominant wind direction corresponds to a flow from the north-northwest, which is also the wind sector with the strongest wind velocities observed during the measurement period. Although the wind rose created with the lidar data is consistent with those obtained from the masts, it shows a higher percentage of southerly winds than on the masts ME1 or MW1. This may be due to the particular location of the scanned area, which is on the north side of the junction of the Bjørnafjord with another fjord. In Figure 4, the percentage of samples associated with easterly winds is noticeably low, for which the majority of the lidar data were characterized by a low signal-to-noise ratio, such that easterly winds are under-represented in the dataset considered. Consequently, Figure 4 does not provide a complete description of the wind conditions in the fjord, but demonstrates the consistency between the mean wind velocities and directions recorded simultaneously by the lidars and the anemometers.

We recall that the lidar records are gathered where the scanning beams intersect (Figure 2). If the collocated data from the anemometer C on the mast MW1 are used, the relative difference

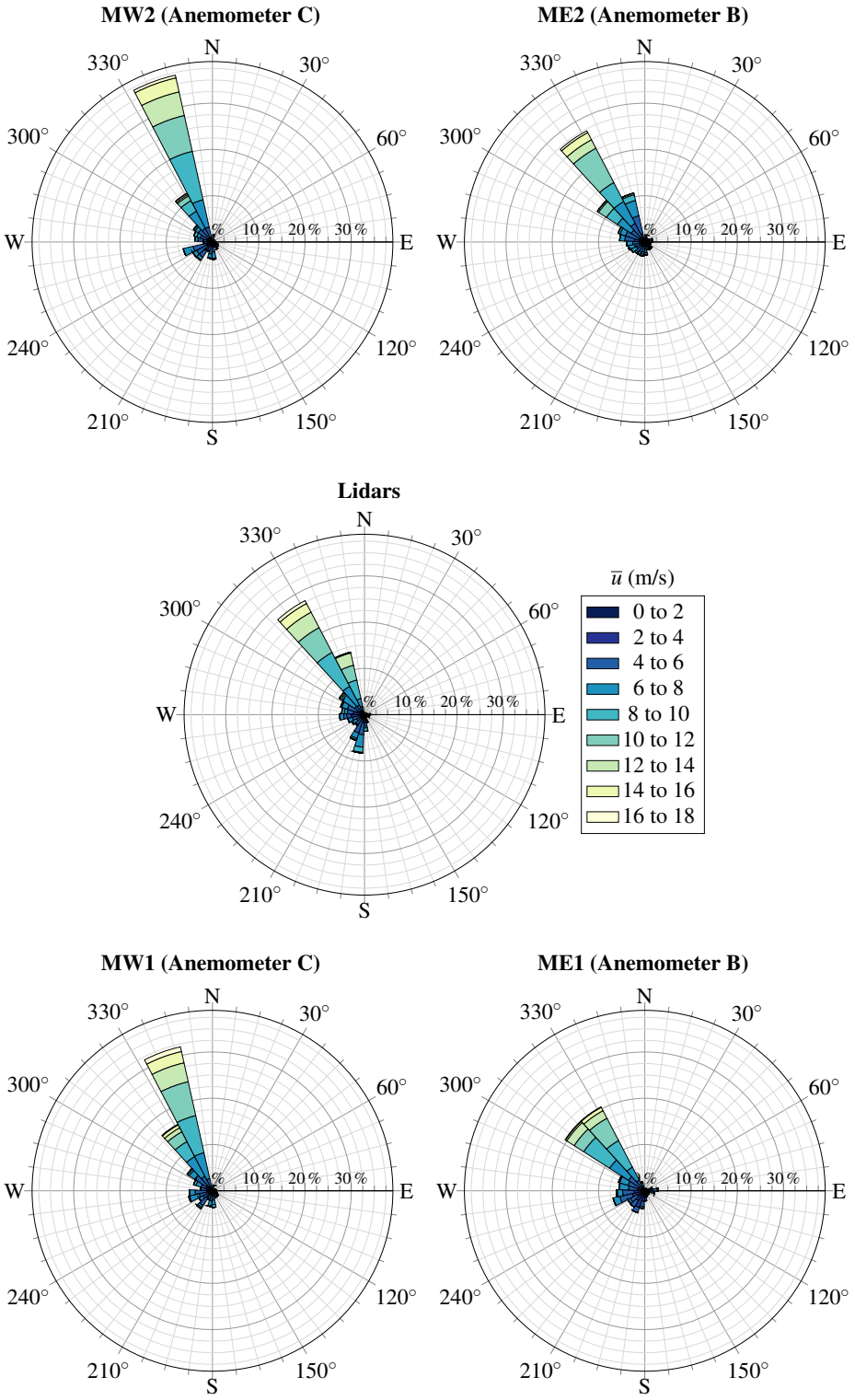


Figure 4: Wind roses obtained using the wind data recorded simultaneously by the sonic anemometers and the lidars, between the 2017-05-18 and 2017-06-22, 33 m (MW1 and MW2), 32 m (ME1 and ME2), and 25 m (lidars) above the ground or sea surface.

for the mean wind velocity is denoted $\epsilon_{\overline{u}}^{\mathrm{W}}$. If the anemometer B on the mast ME1 is used instead, the relative difference is referred to as $\epsilon_{\overline{u}}^{\mathrm{E}}$:

$$\epsilon_{\overline{u}}^{\mathrm{W}} = 1 - \frac{\overline{u}_{\mathrm{MW1}}}{\overline{u}_{\mathrm{lidars}}} \tag{4}$$

$$\epsilon_{\overline{u}}^{\mathrm{E}} = 1 - \frac{\overline{u}_{\mathrm{ME1}}}{\overline{u}_{\mathrm{lidars}}} \tag{5}$$

Using the same notations as in Equations (4) to (5), the relative difference for the mean wind direction $\overline{\Theta}$ is denoted $\epsilon_{\overline{\Theta}}^{\mathrm{W}}$ and $\epsilon_{\overline{\Theta}}^{\mathrm{E}}$, whereas $\epsilon_{\sigma_u}^{\mathrm{W}}$ and $\epsilon_{\sigma_u}^{\mathrm{E}}$ refer to the relative difference for the standard deviation of the along-wind component $\sigma_u$. Only data recorded at $z = 33\,\mathrm{m}$ (MW1) and $z = 32\,\mathrm{m}$ (ME1) are used in Figure 5 because a similar comparison pattern is found using the velocity records at $z = 49\,\mathrm{m}$ (MW1) and $z = 48\,\mathrm{m}$ (ME1). Note that the reference wind direction and mean wind velocity used in Figure 5 are those from the lidar measurements associated with a mean wind velocity above $6\,\mathrm{m\,s^{-1}}$.

Figure 5 shows that the relative error for the mean wind velocity reduces clearly for increasing wind velocities. The main sources of discrepancies are likely the large distance between the masts and the location where the lidar beams intersect as well as the terrain heterogeneity near the masts. For a mean wind direction between 320° and 340° and $\overline{u} \geq 14\,\mathrm{m\,s^{-1}}$ (38 samples), $\epsilon_{\overline{u}}^{\mathrm{W}} \approx 8\,\%$ and $\epsilon_{\overline{\Theta}}^{\mathrm{W}} \approx -2\,\%$, which indicates a remarkable agreement between the lidar data and those recorded by the anemometer C on MW1. For the anemometer B on the mast ME1, a slightly larger relative error is observed in average, with $\epsilon_{\overline{u}}^{\mathrm{E}} \approx 16\,\%$ and $\epsilon_{\overline{\Theta}}^{\mathrm{W}} \approx 3\,\%$. For this wind direction ($320° - 340°$), a positive value of $\epsilon_{\overline{u}}^{\mathrm{E}}$ is expected, since the analysis of the lidar data in Ref. [12, Fig. 17] suggested that the flow from the northwest is decelerated as it approaches the shore where the mast ME1 is installed. This is likely due to the presence of a large island, named Reksteren, located one hundred meters south of the mast ME1, which has a blocking effect on the wind records obtained on the mast ME1.

For a wind direction between 320° and 340° and $\overline{u} \geq 14\,\mathrm{m\,s^{-1}}$, $\epsilon_{\sigma_u}^{\mathrm{W}} \approx -53\,\%$ and $\epsilon_{\sigma_u}^{\mathrm{E}} \approx -37\,\%$. There is also no clear reduction of the data dispersion for increasing mean wind velocities. The low-pass filtering of the velocity data by the lidar instruments is likely the main source of discrepancies. The lidar line-of-sight velocity component is indeed estimated as the weighted average of velocity data measured in the volume where the backscattered light is collected [26]. This volume is stretched along the scanning beam and possesses an axial dimension $L$ much larger than the radial one. Consequently, the length $L$, also called range gate length, is often used alone to describe the spatial dimension of this volume [27]. In the present case, $L \approx 75\,\mathrm{m}$, which is expected to be responsible for an underestimation of ca. 16 % of the turbulence intensity if the scanning beam is perfectly aligned with the wind direction [12].

The volume averaging effect is also clearly visible in Table 2, where the turbulence intensity $I_u$ is estimated with $\overline{u}\,(z = 32\,\mathrm{m}) \geq 10\,\mathrm{m\,s^{-1}}$ and a wind direction between 320° and 340°. Although the turbulence intensity estimates in Table 2 are consistent, the value obtained with the lidar instruments is significantly lower than with the anemometers at $z = 32\,\mathrm{m} - 33\,\mathrm{m}$. The differences between the lidar records and those from the anemometers (fig. 5 and Table 2) do not seem to be explained by the differences in height above ground at which the observations are done.

In the Eurocode [16], wind actions are estimated using a mean return period of 50 years, where a "terrain category 0" corresponds to the sea or a coastal area exposed to the open sea and is associated with a roughness length $z_0 = 0.003\,\mathrm{m}$. For a calm open sea surface, a lower roughness length is expected, with values ranging from $0.0001\,\mathrm{m}$ to $0.0003\,\mathrm{m}$ [28, 29]. For $z_0 = 0.0002\,\mathrm{m}$, Equation (2) leads to $I_u = 0.08$ at a height of 33 m above ground, which is in agreement with the values displayed in Table 2. The larger turbulence intensity recorded on MW1 is expected since, for a northwestern wind, the mast is located downstream of the top of Ospøya (Figure 2). The

presence of multiple sea-land discontinuities some kilometres on the north side and north-west side of Ospøya seems, however, to have a limited influence on the turbulence intensity recorded by the mast MW2, for which $I_u \approx 0.08$ at $z = 33\,\mathrm{m}$.

However, the application of eq. (2) may not always be appropriate at a sea-land discontinuity. In Ref. [30, Eq. 2c], the turbulence intensity was studied on the western tip of the island Frøya. Using their Equation (2c) with $z = 32\,\mathrm{m}$ and $\overline{u}(z = 10\,\mathrm{m}) = 10\,\mathrm{m\,s^{-1}}$, one gets $I_u \approx 0.07$, which is lower than estimated with the anemometers in Table 2.

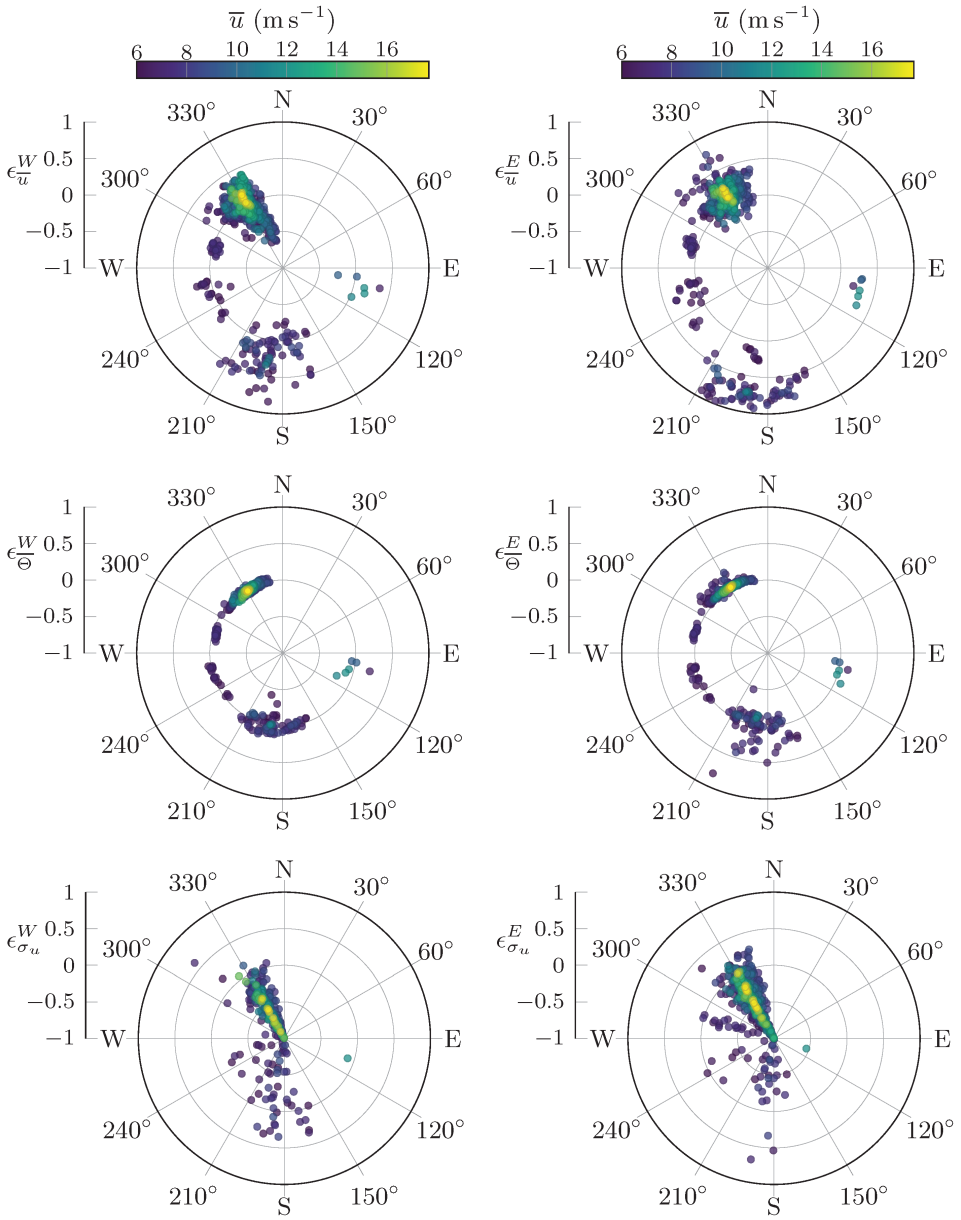


Figure 5: Relative difference for the mean wind velocity $\overline{u}$, the mean wind direction $\overline{\Theta}$ and $\sigma_u$ between the lidar data and the sonic anemometer measurements on the mast MW1 at $z = 33\,\mathrm{m}$ above ground (left panels) and on the mast ME1 at $z = 32\,\mathrm{m}$ above ground (right panels). The dataset comprises 830 samples of 10 min duration.

Table 2: Turbulence intensity estimated from the lidar and anemometer data collocated in time, for a wind direction between 320° and 340° and $\overline{u} > 10\,\mathrm{m\,s^{-1}}$. Average values of the turbulence intensity are derived using a number of samples N.

| Sensor | Lidars ($z = 25\,\mathrm{m}$) | MW1 ($z = 33\,\mathrm{m}$) | MW2 ($z = 33\,\mathrm{m}$) | ME1 ($z = 32\,\mathrm{m}$) | ME2 ($z = 32\,\mathrm{m}$) |
|---|---|---|---|---|---|
| $I_u$ | $0.05 \pm 0.02$ | $0.11 \pm 0.02$ | $0.08 \pm 0.01$ | $0.08 \pm 0.01$ | $0.09 \pm 0.02$ |
| $N$ | 255 | 160 | 126 | 41 | 144 |

## 4. Influence of the local topography on the turbulence characteristics

As suggested in section 3, the local topography around the masts is likely a significant source of discrepancies between the anemometer and lidar data. It is investigated more in details in the present section using the anemometer records alone. The measurement period selected is, therefore, extended from the beginning of May to the end of June, i.e. without restriction with respect to the data availability of the lidar records. Figure 6 shows that the 10 min mean incidence angle recorded by the anemometer B on each mast deviates significantly from 0°. Note that the mean incidence angle is found to be positive when the flow comes from the sea and negative when it comes from the land. Figure 6 shows that the four masts are located in a complex terrain, close to a sea-land discontinuity characterized by both a roughness change and an abrupt elevation difference, generating an internal boundary layer (IBL) with increased shear [4, 31, 32]. The determination of the minimum measurement height above which the anemometers are monitoring wind conditions representative of the middle of the fjord is not straightforward and cannot rely on change-of-roughness models only. The influence of the local topography and the vegetation on the turbulence characteristics estimated from the masts is here investigated using a comparison with values found in the literature in both flat and complex terrains. For the sake of brevity, only anemometer records with a wind direction ranging from 320° to 340° and a mean wind velocity bounded between $12\,\mathrm{m\,s^{-1}}$ and $16\,\mathrm{m\,s^{-1}}$ at $z = 48\,\mathrm{m}$ or $z = 49\,\mathrm{m}$ are considered. This excludes samples characterized by a strongly non-neutral atmospheric condition.

In Table 3, the friction velocity is estimated as advised in Ref. [33]:

$$u_* = \left(\overline{u'w'}^2 + \overline{v'w'}^2\right)^{1/4} \tag{6}$$

Table 3 shows some of the fundamental single-point turbulence characteristics estimated on each sonic anemometer, after application of the double rotation technique. The ratios $\sigma_w/\sigma_u$ and $\sigma_v/\sigma_v$ estimated on ME1 are consistent with those estimated in flat and homogeneous terrains [34], with the value advised in the Eurocode [16] or with those obtained in a coastal area [35, 36]. The ratio $\sigma_v/\sigma_u$ is also found to agree well with the one estimated using the lidar data [12]. Note that if the double rotation technique is not applied, the turbulence characteristics estimated on the mast ME1 are similar to those listed in Ref. [5], where a met mast was located near a sea-land discontinuity on the west coast of France.

The turbulence statistics from the three other masts (Table 3) are associated with values different than observed in the literature for homogeneous terrain and show similarities with those observed in mountainous terrains [37, 38]. Once again, this indicates that for the wind conditions considered here, observational data from the masts ME2, MW1 and MW2 cannot be directly employed to characterize the flow at the middle of the fjord. It should be noted that at the lowest level on the mast ME2, up to 16 % of the samples selected are detected as non-stationary because the anemometer measures a flow significantly disturbed by the surrounding canopy.

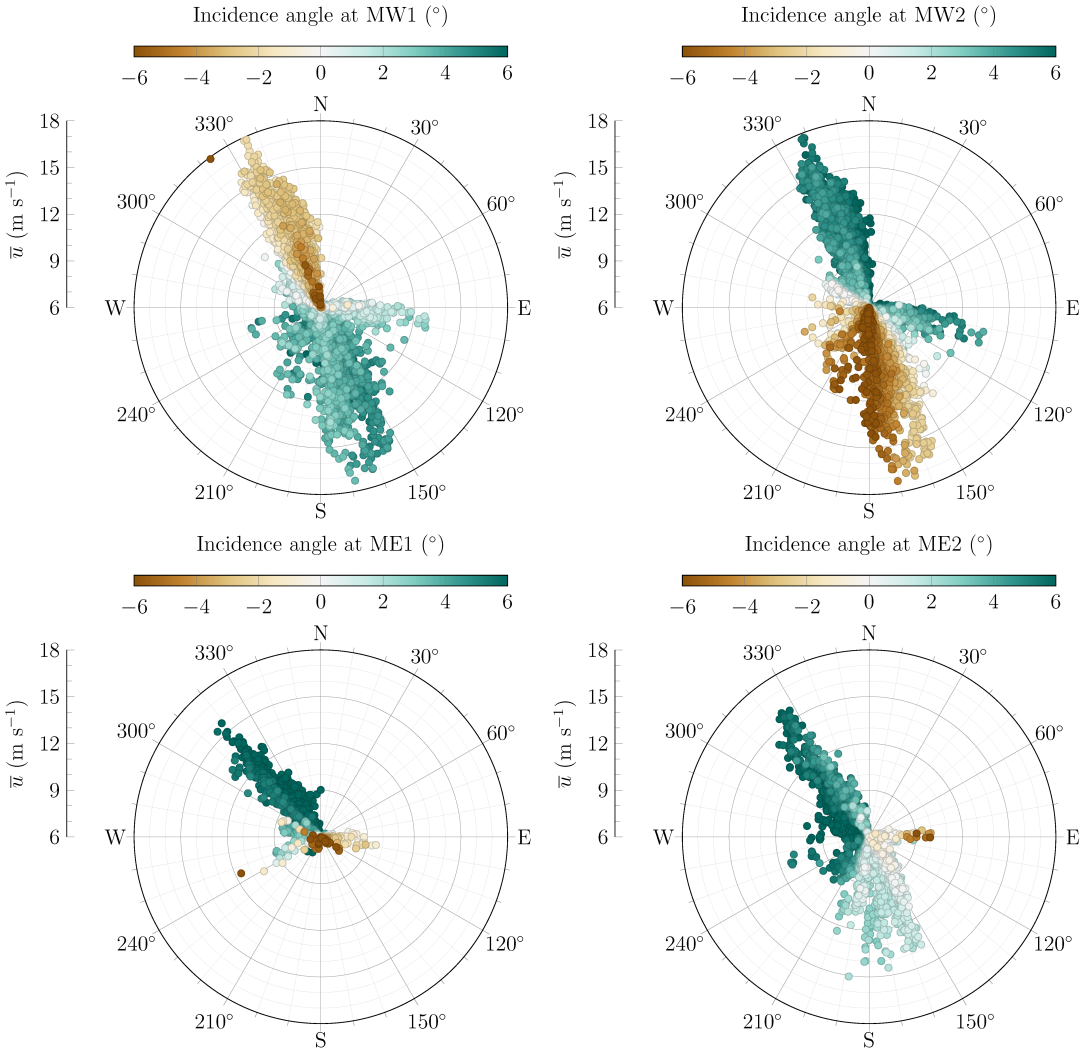


Figure 6: Wind roses showing the mean wind velocity and the incidence angle recorded on the anemometer B on each met-mast for $\overline{u} \geq 6\,\mathrm{m\,s^{-1}}$ from the 2016-05-01 to 2016-07-01.

The turbulence characteristics estimated after application of the double rotation algorithm show only minor differences with those obtained with the SPF technique, which are not displayed here for the sake of brevity. In the Cartesian coordinate system, on the mast ME1, the average wind incidence angle is equal to 6.4° at the highest level. For the masts ME2, MW1 and MW2, the incidence angles at the highest boom are 5.6°, −2.0° and 5.1°, respectively. After application of the SPF algorithm , the incidence angle in the streamline coordinate system is 0.7°, −3.8°, 1.6° and 0.7° for the masts ME1, ME2, MW1 and MW2, respectively. The SPF algorithm does not necessarily succeed in fitting the best plane such that $\overline{w} = 0\,\mathrm{m\,s^{-1}}$. This is likely because the terrain is clearly different from the "gently sloping" case described in Ref. [23]. In fact, the complexity of the topography investigated here is such, that it cannot be reduced to the case of a two-dimensional sloping terrain. Even though the wind sector ranges from 320° to 340° only, there exists a multitude of mean streamline coordinate systems from which the turbulence characteristics from the middle of the fjord cannot be easily derived.

Table 3: Number of samples (N), percentage of non stationary samples (NS), single-point turbulence statistics and associated standard deviation at the mast ME1, for a wind direction between 320° and 340° and a wind velocity between $12\,\mathrm{m\,s^{-1}}$ and $16\,\mathrm{m\,s^{-1}}$ at $z = 48\,\mathrm{m}$ or $z = 49\,\mathrm{m}$. Data outside the 1st and 99th percentile are considered as outliers and removed.

| Mast | N | z (m) | NS (%) | $\sigma_w/u_*$ | $\sigma_v/u_*$ | $\sigma_u/u_*$ | $\sigma_w/\sigma_u$ | $\sigma_v/\sigma_u$ |
|---|---|---|---|---|---|---|---|---|
| ME1 | 130 | 48 | 2 | $1.13 \pm 0.12$ | $1.41 \pm 0.21$ | $1.93 \pm 0.19$ | $0.59 \pm 0.06$ | $0.73 \pm 0.09$ |
| | | 32 | 0 | $1.12 \pm 0.10$ | $1.48 \pm 0.21$ | $1.98 \pm 0.16$ | $0.57 \pm 0.05$ | $0.75 \pm 0.08$ |
| | | 13 | 0 | $1.04 \pm 0.05$ | $1.55 \pm 0.14$ | $1.93 \pm 0.10$ | $0.54 \pm 0.04$ | $0.80 \pm 0.06$ |
| ME2 | 94 | 48 | 1 | $1.98 \pm 0.60$ | $2.24 \pm 0.67$ | $2.49 \pm 0.78$ | $0.81 \pm 0.08$ | $0.91 \pm 0.11$ |
| | | 32 | 0 | $2.16 \pm 0.55$ | $3.26 \pm 0.81$ | $3.16 \pm 0.74$ | $0.69 \pm 0.06$ | $1.04 \pm 0.11$ |
| | | 13 | 16 | $1.27 \pm 0.08$ | $1.32 \pm 0.09$ | $1.81 \pm 0.07$ | $0.71 \pm 0.05$ | $0.73 \pm 0.06$ |
| MW1 | 220 | 49 | 4 | $1.64 \pm 0.28$ | $2.11 \pm 0.41$ | $2.54 \pm 0.42$ | $0.65 \pm 0.07$ | $0.83 \pm 0.13$ |
| | | 33 | 3 | $1.43 \pm 0.18$ | $2.11 \pm 0.37$ | $2.81 \pm 0.34$ | $0.51 \pm 0.05$ | $0.75 \pm 0.10$ |
| MW2 | 145 | 49 | 4 | $1.36 \pm 0.16$ | $1.70 \pm 0.28$ | $1.89 \pm 0.18$ | $0.72 \pm 0.06$ | $0.90 \pm 0.12$ |
| | | 49 | 5 | $1.61 \pm 0.31$ | $1.97 \pm 0.47$ | $2.25 \pm 0.38$ | $0.72 \pm 0.06$ | $0.87 \pm 0.13$ |
| | | 33 | 3 | $1.41 \pm 0.19$ | $1.87 \pm 0.35$ | $2.06 \pm 0.26$ | $0.68 \pm 0.06$ | $0.91 \pm 0.12$ |

## 5. Conclusions

Wind velocity records obtained on the shores of a wide fjord in May and June 2016 from four met-masts are compared to wind data obtained in the middle of the fjord during the same period by synchronized long-range lidars located on the seaside. The data analysis of this unique set-up shows that the mean wind velocity and direction recorded by the lidars and sonic anemometers agree well for a limited number of wind sectors only. Most of the time, the mean statistics and turbulence characteristics recorded on the masts are significantly affected by the local topography.

In the second part of the study, wind records from the anemometers were investigated alone, considering a mean wind velocity from $12\,\mathrm{m\,s^{-1}}$ to $16\,\mathrm{m\,s^{-1}}$ at $z = 48\,\mathrm{m}$ or $z = 49\,\mathrm{m}$ and a wind direction ranging from 320° to 340°. The anemometer measurements on three of the four masts lead to one-point turbulence characteristics that are not representative of flat and homogeneous terrain. For a wind direction between 320° and 340°, the mast ME1 is less affected by the topography than the others for two reasons: (1) it is located directly on the sea-land discontinuity, which is flatter than for the masts MW1 and MW2; (2) contrary to the mast ME2, it is not located downstream of trees for the wind sector selected. The unavoidable influence of the local topography on the wind data recorded by the anemometers on land encourages the combined use of remote sensing technology and land-based sensors to properly characterize the wind conditions in a wide fjord.


## Acknowledgements

The measurements were performed with the support from the Norwegian Public Road Administration (NPRA). The authors are grateful to Benny Svardal from Christian Mikkelsen Research, to Jakob Mann, Michael Courtney, Guillaume Lea, Claus Brian Munk Pedersen, Søren William Lund from the Technical University of Denmark and Jarle Berge from the University of Stavanger for their contributions and assistance in the lidar measurement campaign. François Beauducel is also acknowledged for writing the original function facilitating the use of SRTM digital elevation model data files (https://www.mathworks.com/matlabcentral/fileexchange/36379-readhgt–import-download-nasa-srtm-data-files—hgt-).

## References


[1] Norwegian Ministry of Transport and Communication 2013 National Transport Plan 2014 2023. Report to Storting (White Paper) Summary
[2] Turnipseed A, Anderson D, Blanken P, Baugh W and Monson R 2003 *Agric. For. Meteorol.* **119** 1–21
[3] Cheynet E, Jakobsen J B, Snæbjörnsson J, Reuder J, Kumer V and Svardal B 2017 *J. Wind Eng. Ind. Aerodyn.* **161** 17–26
[4] Peterson E W, Kristensen L and Su C C 1976 *Q. J. Royal Meteorol. Soc.* **102** 857–869
[5] Sacré C 1981 *Bound.-Layer Meteorol.* **21** 57–76
[6] Jensen N O 1978 *Bound.-Layer Meteorol.* **15** 95–108
[7] Berg J, Mann J, Bechmann A, Courtney M and Jørgensen H E 2011 *Bound.-Layer Meteorol.* **141** 219–243
[8] Cheynet E, Jakobsen J B, Snæbjörnsson J, Mikkelsen T, Sjöholm M, Mann J, Hansen P, Angelou N and Svardal B 2016 *Exp. Fluids* **57** 184 ISSN 1432-1114
[9] Emeis S, Harris M and Banta R M 2007 *Meteorol Z.* **16** 337–347
[10] Sathe A and Mann J 2013 *Atmospheric Meas. tech.* **6** 3147–3167
[11] Reitebuch O 2012 Wind lidar for atmospheric research *Atmospheric Phys.* Research Topics in Aerospace (Springer) pp 487–507 ISBN 978-3-642-30182-7
[12] Cheynet E, Jakobsen J B, Snæbjörnsson J, Mann J, Courtney M, Lea G and Svardal B 2017 *Remote Sens.* **9** 977
[13] Ágústsson H 2018 E39, brukrysninger Hordaland. Statusrapport 6 for vindmlinger pr desember 2017 [E39, bridge-crossing Hordaland. Status report 6 for wind measurements in december 2017 ] (in Norwegian) Tech. Rep. no. KVT/HÁ/2018/R007 Kjeller Vindteknikk, Kjeller, Norway
[14] Vasiljević N, Lea G, Courtney M, Cariou J P, Mann J and Mikkelsen T 2016 *Remote Sens.* **8** 896
[15] Kaimal J C and Finnigan J J 1994 *Atmospheric boundary layer flows: their structure and measurement* (Oxford University Press)
[16] EN 1991-1-4 2005 Eurocode 1: Actions on structures–part1-4: General actions-wind actions
[17] Högström U 1988 *Bound.-Layer Meteorol* **42** 55–78 ISSN 1573-1472
[18] Lumley J L and Panofsky H A 1964 *The structure of atmospheric turbulence* (John Wiley & Sons)
[19] Finnigan J 1983 *J. Fluid Mech.* **130** 241–258
[20] Zeman O and Jensen N O 1987 *Q. J. Royal Meteorol. Soc..* **113** 55–80
[21] Finnigan J, Raupach M, Bradley E F and Aldis G 1990 *Bound.-Layer Meteorol.* **50** 277–317
[22] Paw U K T, Baldocchi D D, Meyers T P and Wilson K B 2000 *Bound.-Layer Meteorol.* **97** 487–511 ISSN 1573-1472
[23] Wilczak J M, Oncley S P and Stage S A 2001 *Bound.-Layer Meteorol.* **99** 127–150
[24] McMillen R T 1988 *Bound.-Layer Meteorol.* **43** 231–245
[25] Bendat J and Piersol A 2011 *Random Data: Analysis and Measurement Procedures* Wiley Series in Probability and Statistics (Wiley) ISBN 9781118210826
[26] Frehlich R, Hannon S M and Henderson S W 1998 *Bound.-Layer Meteorol* **86** 233–256 ISSN 1573-1472
[27] Mann J, Cariou J P, Courtney M, Parmentier R, Mikkelsen T, Wagner R, Lindelöw P, Sjöholm M and Enevoldsen K 2009 *Meteorol. Z.* **18** 135–140
[28] Smith S D 1980 *J. Phys. Oceanogr.* **10** 709–726
[29] Wieringa J 1992 *J. Wind Eng. Ind. Aerodyn.* **41** 357–368
[30] Andersen O J and Løvseth J 2006 *Marine Structures* **19** 173 – 192 ISSN 0951-8339
[31] Elliott W P 1958 *Eos Trans. Am. Geophys. Union* **39** 1048–1054
[32] Panofsky H A and Townsend A 1964 *Q. J. Royal Meteorol. Soc.* **90** 147–155
[33] Weber R 1999 *Bound.-Layer Meteorol* **93** 197–209 ISSN 0006-8314
[34] Solari G and Piccardo G 2001 *Probabilistic Eng. Mech.* **16** 73–86
[35] Iwatani Y and Shiotani M 1984 *J. Wind Eng. Ind. Aerodyn.* **17** 147 – 157
[36] Smedman A S 1991 *J. Atmos. Sci.* **48** 856–868
[37] Founda D, Tombrou M, Lalas D and Asimakopoulos D 1997 *Bound.-Layer Meteorol.* **83** 221–245
[38] Helgason W and Pomeroy J W 2012 *J. Appl. Meteorol. Climatol.* **51** 583–597